

Operational Coordination Optimization of Electricity and Natural Gas Networks Based on Sequential Symmetrical Second-order Cone Programming

Liang Min, Chengwei Lou, Jin Yang, *Senior Member, IEEE*, James Yu, and Zhibin Yu

Abstract—The variable and unpredictable nature of renewable energy generation (REG) presents challenges to its large-scale integration and the efficient and economic operation of the electricity network, particularly at the distribution level. In this paper, an operational coordination optimization method is proposed for the electricity and natural gas networks, aiming to overcome the identified negative impacts. The method involves the implementation of bi-directional energy flows through power-to-gas units and gas-fired power plants. A detailed model of the three-phase power distribution system up to each phase is employed to improve the representation of multi-energy systems to consider real-world end-user consumption. This method allows for the full consideration of unbalanced operational scenarios. Meanwhile, the natural gas network is modelled and analyzed with steady-state gas flows and the dynamics of the line pack in pipelines. The sequential symmetrical second-order cone programming (SS-SOCP) method is employed to facilitate the simultaneous analysis of three-phase imbalance and line pack while accelerating the solution process. The efficacy of the operational coordination optimization method is demonstrated in case studies comprising a modified IEEE 123-node power distribution system with a 20-node natural gas network. The studies show that the operational coordination optimization method can simultaneously minimize the total operational cost, the curtailment of installed REG, the voltage imbalance of three-phase power system, and the overall carbon emissions.

Index Terms—Operational coordination, multi-energy system, power-to-gas, electricity network, natural gas network, second-order cone programming.

Manuscript received: October 3, 2023; revised: March 19, 2024; accepted: September 3, 2024. Date of CrossCheck: September 3, 2024. Date of online publication: October 4, 2024.

The work was supported by the Engineering and Physical Sciences Research Council (EPSRC, UK) in project “Street2Grid – an electricity blockchain platform for P2P energy trading” (No. EP/S001778/2).

This article is distributed under the terms of the Creative Commons Attribution 4.0 International License (<http://creativecommons.org/licenses/by/4.0/>).

L. Min is with Power Grid Dispatching and Control Branch Company of NARI Technology Co., Ltd., Nanjing, China (e-mail: minliang@sgepri.sgcc.com.cn).

C. Lou (corresponding author) is with the College of Information and Electrical Engineering, China Agricultural University, Beijing, China (e-mail: chengwei.lou@cau.edu.cn).

J. Yang is with the James Watt School of Engineering, University of Glasgow, Glasgow G12 8QQ, UK (e-mail: Jin.Yang@glasgow.ac.uk).

J. Yu is with Scottish Power Energy Network, Glasgow G2 5AD, UK (e-mail: james.yu@spenergynetworks.co.uk).

Z. Yu is with the Department of Mechanical and Aerospace Engineering, University of Liverpool, Liverpool, UK (e-mail: Zhibin.Yu@liverpool.ac.uk).

DOI: 10.35833/MPCE.2023.000750

I. INTRODUCTION

THE penetration of renewable energy generation (REG) has been on a continuous upward trajectory, driven by the imperative to mitigate the adverse effects of environmental deterioration. Consequently, there is a global tendency towards a transformation in the energy sector, with the aim of transitioning towards a low-carbon economy. However, the integration of REG encounters a considerable obstacle due to the limitations of current power grids in managing inherent characteristics of REG, including its intermittent nature, counter-peak demand impact, and the phenomenon of reverse power flow [1]. Therefore, it is evident that both power network operators and individual customers would benefit from a reduction in curtailment and waste of renewable energy resources, thus allowing for more effective utilization of these resources for further carbon emission reduction.

One way to facilitate this utilization is by power-to-gas (P2G) units [2]. During periods of low electricity consumption, excess electricity from the REG can be converted to natural gas by P2G units. The natural gas is then injected into the pipelines of the natural gas network, thus storing the abundant renewable energy in the form of gas [3]. Consequently, in conjunction with the gas-fired power plants (GFPPs) that utilize natural gas as fuel to generate electricity for the power network, P2G units can facilitate the formation of a closed loop of energy conversion within an electricity-natural gas multi-energy system (ENG-MES) [4]. The coupling of electricity and natural gas has traditionally been considered at the transmission level, primarily due to the predominant usage of GFPPs. However, with the promotion of distributed REGs, the distribution-level integrated electricity and natural gas networks consists of small or micro GFPPs. Emerging P2G units and distributed REGs can be utilized to couple the natural gas network with the power distribution system via GFPPs and P2G units [4]-[6].

Multiple studies have delved into modeling integrated energy systems. In [7], an optimal dispatch model for the electricity and natural gas networks is proposed, where bi-directional energy flow is considered. The Wendorff difference form is adopted to linearize gas flow constraints. In [8], a day-ahead operational optimization of the decentralized deci-

sion-making method is proposed for an integrated electricity and natural gas network with P2G. Reference [9] proposes a distributionally robust chance-constrained model for the optimal power-gas flow problem with varying wind power. The proposed model is designed to adjust the flexible resources in both systems for uncertainty mitigation. In a further contribution to the field, [10] proposes a mixed-integer nonlinear unit commitment model with non-convex nonlinear gas flow equations. An enhanced convex relaxation is implemented to make the model tractable while simultaneously obtaining high-quality solutions. In [11], a combined power, heat, and natural gas dispatch model is established to investigate the network flexibility with the nonconvex flow dynamics of gas accounted for in a computationally efficient manner.

However, the aforementioned models of either the power system or the natural gas network are over-simplified. In [7], [8], [10], and [11], although the line pack in pipelines is considered, the physical constraints of the power system are simplified with lossless ideal DC power flow. In [9], the constraints do not include voltage limits of the power system. Furthermore, no existing research adopts a detailed three-phase model of power systems within a multi-energy system (MES).

This imbalance is not merely a theoretical concern; rather, it reflects real-world operational challenges within power distribution networks. As evidenced by the IEEE distribution test node feeders, unbalanced conditions across the three phases are a prevalent phenomenon [12]. The negative impacts of phase imbalances on the operation of the power system include, but are not limited to: ① additional network investment costs; ② extra energy losses; ③ nuisance tripping; and ④ damages to induction motors. The integration of REG may be impeded by an imbalance in the three-phase power system, which can result in voltage fluctuations and the derating of power converters used in both wind and photovoltaic (PV) systems. Furthermore, the mismatch in phase voltages can lead to asymmetric power flow, which in turn can exacerbate power quality issues such as harmonics and flicker. Such power quality issues have the potential to disrupt the stable operation of wind power and PV, leading to their disconnection from the grid during periods of high demand or volatility. Therefore, the MES operator needs to tackle the issue of a three-phase imbalance in the power system.

From the perspective of operation optimization, convex optimization, also known as convex optimal power flow (OPF) is widely used for three-phase unbalanced power systems. This includes second-order cone programming (SOCP) OPF and semidefinite programming (SDP) OPF. A single-phase OPF is derived as a mixed-integer second-order cone programming (MI-SOCP) by [13] with the objective of achieving a global optimal solution. In [14], a three-phase unbalanced OPF based on a quasi-Newton method is proposed as a means of optimizing three-phase unbalanced power systems. Reference [15] proves that a bus-injection model SDP (BIM-SDP) can obtain the global optimal solution to the original non-convex OPF problem. Reference [16] indicates that the branch-flow model SDP (BFM-SDP) can im-

prove the stability of the BIM-SDP. In [17], the stability and accuracy are enhanced by substituting the existing BFM-SDP model with a symmetrical SDP algorithm. However, as SDP algorithm retains the nonlinearity within the constraints of power flow, this method results in significant computational demands, rendering it unsuitable for real-time implementation. The complexity and computational intensity of SDP solutions pose challenges to the employment in large-scale power systems. Additionally, the SDP algorithm may lack robustness in the presence of uncertainties and disturbances [18]. In contrast, SOCP offers an achievement of the trade-off between solving efficiency and global accuracy. By converting the constraints of power flow into a conic form, SOCP can not only retain part of the nonlinearity but also more realistically model the three-phase unbalanced power system. Several recent studies have utilized SOCP as a convex optimization technique to formulate and solve a range of issues related to the operation of power distribution systems [19]. Besides, SOCP overlooks the coupling between three phases, leading to varying degrees of inaccuracy in the optimization results. In [20], a model of symmetrical SOCP is introduced for the optimization of three-phase unbalanced systems. It is proven that symmetrical SOCP can minimize errors arising from decompositions and maintain the complex relationships within the three-phase power systems.

Meanwhile, convex optimization has started to be applied in modeling natural gas networks. The Weymouth equation, which explains how gas flows and nodal pressures are related, is non-convex, proving to be a challenge for finding the optimal operation solution. The computational advantages of convex optimization are utilized to replace the Weymouth equation with more relaxed but simpler constraints. Reference [21] integrates an SOCP relaxation of a non-convex nonlinear gas flow model considering the line pack in the pipeline to linearize the gas flow balance equations. In [22], the nonconvex Weymouth gas flow equations of the natural gas network are convexified as quadratic constraints, while the convex relaxation is performed on the nonconvex branch flow equations of the power system. Reference [23] reformulates the natural gas network as a single-level mixed-integer SOCP. In [24], SOCP relaxation is utilized in day-ahead optimization for an integrated gas-electricity energy system. Using sequential SOCP, the optimal scheduling of a hydrogen-blended integrated electricity-natural gas network (ENGN) is presented in [25]. This method effectively balances computational efficiency and solution quality, demonstrating a 91% improvement in computational efficiency compared with general nonlinear solvers.

In summary, the symmetrical SOCP has proven efficient in the optimization of three-phase unbalanced power systems. Concurrently, the sequential SOCP has shown effectiveness in the line pack dynamics of natural gas networks. However, there remains a gap in addressing the combined optimization of ENG-MES, particularly when simultaneously considering the three-phase imbalance in electricity and line pack dynamics.

Accordingly, this paper aims to bridge this gap by integrating symmetrical SOCP with sequential SOCP, thereby cou-

pling the dynamics of electricity and natural gas for the operational optimization of ENG-MES. By incorporating the detailed three-phase modeling of unbalanced power systems with natural gas networks, our method can facilitate a comprehensive understanding of the interdependencies between electricity and natural gas networks. The contributions of this paper are presented as follows.

1) A holistic operational coordination optimization method is proposed for ENG-MES, with bi-directional energy flows through P2G units and GFPPs. The closed energy conversion loop formed within the MES can fulfill a complete carbon cycle. A comprehensive model integrating three-phase unbalanced power systems with natural gas networks is built. In the proposed model, both the phase imbalance of the power distribution system and the line pack dynamics of the pipelines are considered simultaneously.

2) A novel method, namely a sequential symmetrical SOCP (SS-SOCP) method, is introduced. This method leverages symmetrical SOCP for power constraints and sequential SOCP for natural gas constraints. The purpose of this method is to convert the original non-convex nonlinear model into a solvable model. Consequently, the coupling of MES can be analyzed together with the three-phase imbalance issue of the power grid and the line pack dynamics of the pipelines.

3) A modified IEEE 123-node power distribution system with a 20-node natural gas network is established, which can be used as a future benchmark for MES. The operational cost, reduced curtailment of the installed REGs, improved voltage imbalance of the three-phase power system, and lower overall carbon emissions are achieved.

II. INTERDEPENDENCE BETWEEN ELECTRICITY NETWORK AND NATURAL GAS NETWORK

The interdependency between the electricity network and the natural gas network is illustrated, as shown in Fig. 1. The P2G unit, producing natural gas from electricity, serves as a gas source in the natural gas network and as a flexible electric load in the electricity network. The GFPP, generating electricity from the combustion of natural gas, works as a power source in the electricity network and as a gas load in the natural gas network. These two synergies physically link the ENG-MESs.

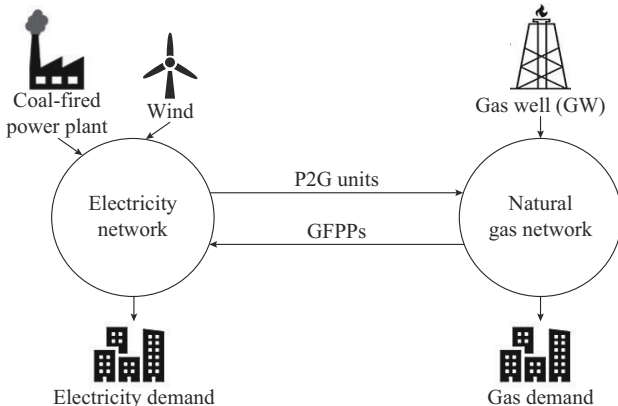


Fig. 1. Interdependence between electricity network and natural gas network.

The P2G can largely contribute to the decarbonization of ENG-MES and the integration of REG, as the application of P2G units can fully explore the following advantages of low-carbon technologies.

Firstly, the natural gas, produced by P2G, is carbon neutral. In the first stage of P2G, hydrogen (H_2) is produced by the technology of electrolysis. Then, the hydrogen is reacted with carbon dioxide (CO_2) to produce methane (CH_4). During the conversion from electricity to natural gas, the same amount of CO_2 produced by burning the natural gas will be captured from the air and consumed. Therefore, the natural gas produced by P2G is carbon neutral and the overall carbon emission of the ENGN can be reduced.

Secondly, because of the dynamic line pack of the pipelines, the excessive electricity from REG can be converted by P2G into natural gas, which can then be stored in the pipelines. Thus, the natural gas network can serve as an energy storage system for the electricity network.

Compared with traditional battery energy storage, P2G units have the advantages of larger storage capacity (the whole gas network) and higher energy conversion efficiency (60%-70%). As a result, a P2G unit can work as a large-capacity controllable load in the electricity network to consume the excess electricity from REG without being constrained by the capacity of conventional battery energy storage. The produced natural gas can be directly utilized by gas loads or GFPPs. Meanwhile, as both the GFPPs and the P2G units have the characteristics of fast response, they can be deployed as coupling points to realize the bidirectional energy flows in integrated ENGN.

III. OPTIMAL OPERATIONAL COORDINATION OPTIMIZATION

A. Objective Functions

The proposed optimal operational coordination optimization aims at minimizing the total operational cost F_{Cost} , the curtailment of wind power generation F_{Wind} , and the carbon emission F_C .

$$F = \min \sum_{t=0}^T (W_{Cost} F_{Cost} + W_{Wind} F_{Wind} + W_C F_C) \quad (1)$$

$$F_{Cost} = \sum_{t=0}^T \left(C^{grid} P_t^{grid} + \sum_{u=1}^U C^{gas} g_{u,t} \right) \quad (2)$$

$$F_{Wind} = \sum_{t=0}^T \sum_{k=1}^K (P_{k,t}^{Avail} - P_{k,t}^{Wind}) \quad (3)$$

$$F_C = \sum_{t=0}^T \left(\alpha^{grid} P_t^{grid} + \sum_{u=1}^U \alpha^{gas} g_{u,t} - \alpha^{P2G} P_t^{P2G} \right) \quad (4)$$

where W_{Cost} , W_{Wind} , and W_C are the weight coefficients of objectives; C^{grid} and C^{gas} are the costs of electricity and natural gas, respectively; P_t^{grid} is the electric power from the higher level (upstream) power grid at time t ; $g_{u,t}$ is the natural gas supply of the GW unit u at time t ; T , K , and U are the total amounts of time, wind power unit, and GW unit, respectively. $P_{k,t}^{Avail}$ is the available wind power generation of the wind power unit k at time t ; $P_{k,t}^{Wind}$ is the actual power output of the wind power unit k at time t ; α^{grid} , α^{gas} , and α^{P2G} are the carbon emission rates of electric power from upstream pow-

er grid, natural gas supply, and the power used by the P2G unit, respectively; and P_t^{P2G} is the power consumed by the P2G unit at time t .

The weighted sum method (WSM) [26] is utilized in the multi-objective optimization problem. The weight coefficients are derived as:

$$W_{Cost} = \frac{\rho_{Cost}}{f_{Orig}^{Cost}} \quad (5)$$

$$W_{Wind} = \frac{\rho_{Wind}}{f_{Orig}^{Wind}} \quad (6)$$

$$W_C = \frac{\rho_C}{f_{Orig}^C} \quad (7)$$

$$\rho_{Cost} + \rho_{Wind} + \rho_C = 1 \quad (8)$$

where f_{Orig}^{Cost} , f_{Orig}^{Wind} , and f_{Orig}^C are the unoptimized original values of F_{Cost} , F_{Wind} , and F_C , respectively; and ρ_{Cost} , ρ_{Wind} , and ρ_C are the weight indexes of the total operational cost, the curtailed wind power generation, and the overall carbon emission, respectively. The sum of ρ_{Cost} , ρ_{Wind} , and ρ_C should always be 1 [27].

B. Three-phase Power System Constraints

Optimization modeling involves using the Kron reduction (KR) method to analyze electricity networks. This method replaces the three-phase four-wire system with three-phase conductor nodes while ensuring that the performance behavior of terminal voltages and currents remains consistent at the desired vertices [28]. In general practices, e. g., Standard IEEE PES test feeders, three-order \mathbf{Z} and \mathbf{Y} matrices are provided for three-phase four-wire systems [29].

The node voltage vectors and related second-order decision variables are defined as:

$$\mathbf{V}_{i,t} = [V_{i,t}^a \quad V_{i,t}^b \quad V_{i,t}^c] \quad (9)$$

$$\mathbf{v}_{i,t} = \mathbf{V}_{i,t} \mathbf{V}_{i,t}^H \quad (10)$$

where $\mathbf{V}_{i,t}$ is the voltage vector of node i at time t ; $V_{i,t}^a$, $V_{i,t}^b$, and $V_{i,t}^c$ are the voltages on phase a , b , and c of node i at time t , respectively; $\mathbf{v}_{i,t}$ is the second-order decision variable for voltage of node i at time t ; and the superscript H indicates the Hermitian transpose.

Similarly, the vectors of current and power and their related second-order decision variables are described as:

$$\mathbf{I}_{ij,t} = [I_{ij,t}^a \quad I_{ij,t}^b \quad I_{ij,t}^c] \quad (11)$$

$$\mathbf{I}_{ij,t} = \mathbf{I}_{ij,t} \mathbf{I}_{ij,t}^H \quad (12)$$

$$\mathbf{S}_{ij,t} = \mathbf{V}_{i,t} \mathbf{I}_{ij,t}^H \quad (13)$$

where $\mathbf{I}_{ij,t}$ is the current vector of branch ij at time t ; $I_{ij,t}^a$, $I_{ij,t}^b$, and $I_{ij,t}^c$ are the currents on phases a , b , and c of branch ij at time t , respectively; $\mathbf{I}_{ij,t}$ is the second-order decision variable of current from node i to node j at time t ; and $\mathbf{S}_{ij,t}$ is the second-order decision variable of power from node i to node j at time t .

Rather than condensing the entire grid states (including voltages, currents, and power) into a singular and large symmetrical matrix variable, the diminutive matrices are utilized in the symmetrical SOCP modelling. The diminutive matrices

typically have the dimensions of 1×1 , 2×2 , and 3×3 .

In (9) and (11), the multi-phase voltage $\mathbf{V}_{i,t}$ and current $\mathbf{I}_{ij,t}$ are represented as vectors. The dimension of the vectors and related matrices of the second-order decision variables are determined by the phase conditions of each branch in the power grid. For example, for the branch from node i to node j , the nodal voltage vectors are defined as $\mathbf{V}_{i,t}$ and $\mathbf{V}_{j,t}$, and the current $\mathbf{I}_{ij,t}$. If node i has three phases, then $\mathbf{V}_{i,t} = [V_{i,t}^a \quad V_{i,t}^b \quad V_{i,t}^c]$. If node j only has phases a and c , then $\mathbf{V}_{j,t} = [V_{j,t}^a \quad V_{j,t}^c]$ and branch ij is a two-phase line with $\mathbf{I}_{ij,t} = [I_{ij,t}^a \quad I_{ij,t}^c]$. As the second-order decision variables are designed using matrices $\mathbf{v}_{i,t} = \mathbf{V}_{i,t} \mathbf{V}_{i,t}^H$, $\mathbf{I}_{ij,t} = \mathbf{I}_{ij,t} \mathbf{I}_{ij,t}^H$ and $\mathbf{S}_{ij,t} = \mathbf{V}_{i,t} \mathbf{I}_{ij,t}^H$, $\mathbf{v}_{i,t}$ is a 3×3 matrix, while $\mathbf{I}_{ij,t}$ and $\mathbf{S}_{ij,t}$ are 2×2 matrices.

The three-phase power distribution system is modelled through the constraints of power flow balance and voltage described as follows.

$$\sum \text{diag}(\mathbf{S}_{ij,t} - \mathbf{Z}_{ij} \mathbf{I}_{ij,t}) + \mathbf{s}_{j,t} + \mathbf{y}_{j,t} \mathbf{v}_{j,t} = \sum \text{diag}(\mathbf{S}_{jk,t}) \quad (14)$$

$$\mathbf{v}_{j,t} = \mathbf{v}_{i,t} - (\mathbf{S}_{ij,t} \mathbf{Z}_{ij}^H + \mathbf{S}_{ij,t}^H \mathbf{Z}_{ij}) + \mathbf{Z}_{ij} \mathbf{I}_{ij,t} \mathbf{Z}_{ij}^H \quad (15)$$

$$\underline{\mathbf{v}}_i \leq \text{diag}(\mathbf{v}_{i,t}) \leq \bar{\mathbf{v}}_i \quad (16)$$

where $\mathbf{s}_{j,t}$ is the nodal power injection at node j at time t ; $\mathbf{y}_{j,t}$ is the nodal shunt admittance; \mathbf{Z}_{ij} is the impedance of branch ij ; $\mathbf{v}_{j,t}$ is the second-order decision variable of voltage at node j at time t ; $\mathbf{S}_{jk,t}$ is the downstream power flow from node j at time t ; and $\underline{\mathbf{v}}_i$ and $\bar{\mathbf{v}}_i$ are the lower and upper limits of voltage at node i , respectively.

In the context of symmetrical SOCP, the term ‘‘symmetrical’’ refers to the symmetrical components, which are denoted as the 012 components. The symmetrical components are utilized to the analysis of three-phase unbalanced power grid. Although the variable matrix in SDP is naturally symmetric, the three-phase components (e. g., $V_{i,t}^a$, $V_{i,t}^b$, $V_{i,t}^c$) are asymmetrical due to the existing imbalances within the three-phase power grid. In this paper, as the three-phase unbalanced power grid are decoupled by the symmetrical component transformation [30], the symmetrical components transformation is employed to mitigate the phase coupling inherent in the three-phase backbones of the power distribution system. Therefore, the constraints listed above need to be reformulated as the symmetrical model.

Through (17) and (18), as the phase components, the three-phase voltages $\mathbf{V}_{i,t}^{abc}$ are converted into symmetrical components.

$$\mathbf{V}_{i,t}^{abc} = \mathbf{A} \mathbf{V}_{i,t}^{012} \quad (17)$$

$$\begin{cases} \mathbf{A} = \begin{bmatrix} 1 & 1 & 1 \\ 1 & a^2 & a \\ 1 & a & a^2 \end{bmatrix} \\ \mathbf{A}^H = \mathbf{A}^{-1} \end{cases} \quad (18)$$

Therefore, the constraints, including power flow balance in (14) and voltage constraints in (15) and (16), are established as:

$$\begin{aligned} \sum \text{diag}(\mathbf{A}(\mathbf{S}_{ij,t}^{012} - \mathbf{z}_{ij,t}^{012} \mathbf{I}_{ij,t}^{012}) \mathbf{A}^H) + \mathbf{s}_{j,t} + \mathbf{y}_{j,t}^{012} \mathbf{v}_{j,t}^{012} = \\ \sum \text{diag}(\mathbf{A} \mathbf{S}_{jk,t}^{012} \mathbf{A}^H) \end{aligned} \quad (19)$$

where $\mathbf{z}_{ij,t}^{012}$ is the symmetrical component of impedance of branch ij at time t .

$$\mathbf{v}_{j,t}^{012} = \mathbf{v}_{i,t}^{012} - \left(\mathbf{S}_{ij,t}^{012} (\mathbf{z}_{ij,t}^{012})^H + (\mathbf{S}_{ij,t}^{012})^H \mathbf{z}_{ij,t}^{012} \right) + \mathbf{z}_{ij,t}^{012} \mathbf{I}_{ij,t}^{012} (\mathbf{z}_{ij,t}^{012})^H \quad (20)$$

$$\mathbf{v}_i \leq \text{diag}(\mathbf{A} \mathbf{v}_{i,t}^{012} \mathbf{A}^H) \leq \bar{\mathbf{v}}_i \quad (21)$$

The symmetric positive semidefinite constraint, requiring the matrix to be positive semidefinite and maintaining a rank-one restriction, is given as:

$$\begin{bmatrix} \mathbf{v}_i^{012} & \mathbf{S}_{ij}^{012} \\ \mathbf{S}_{ij}^{012,H} & \mathbf{I}_{ij}^{012} \end{bmatrix} \succeq 0 \quad i \rightarrow j \quad (22)$$

Using the Sylvester criterion [31], the matrix components are converted to the SOCP constraints expressed as:

$$\left\| \begin{bmatrix} 2\mathbf{v}_{i,t}^{012}(k,l) \\ \mathbf{v}_{i,t}^{012}(k,k) - \mathbf{v}_{i,t}^{012}(l,l) \end{bmatrix} \right\|_2 \leq \mathbf{v}_{i,t}^{012}(k,k) + \mathbf{v}_{i,t}^{012}(l,l) \quad (23)$$

$$\left\| \begin{bmatrix} 2\mathbf{I}_{ij,t}^{012}(k,l) \\ \mathbf{I}_{ij,t}^{012}(k,k) - \mathbf{I}_{ij,t}^{012}(l,l) \end{bmatrix} \right\|_2 \leq \mathbf{I}_{ij,t}^{012}(k,k) + \mathbf{I}_{ij,t}^{012}(l,l) \quad (24)$$

$$\left\| \begin{bmatrix} 2\mathbf{S}_{i,t}^{012}(k,l) \\ \mathbf{v}_{i,t}^{012}(k,k) - \mathbf{I}_{ij,t}^{012}(l,l) \end{bmatrix} \right\|_2 \leq \mathbf{v}_{i,t}^{012}(k,k) + \mathbf{I}_{ij,t}^{012}(l,l) \quad (25)$$

where $\mathbf{v}_{i,t}^{012}(k,l)$, $\mathbf{I}_{ij,t}^{012}(k,l)$, and $\mathbf{S}_{i,t}^{012}(k,l)$ denote the $(k,l)^{\text{th}}$ elements of the matrices $\mathbf{v}_{i,t}^{012}$, $\mathbf{I}_{ij,t}^{012}$, and $\mathbf{S}_{i,t}^{012}$, respectively.

C. Natural Gas Network Constraints

The natural gas network is modelled by applying the steady-state gas flow model considering the line pack in the pipelines.

The gas supply capacity constraint of the GW unit u is given as:

$$0 \leq g_{u,t} \leq \bar{g}_u \quad (26)$$

where \bar{g}_u is the upper limit of the gas supply.

The pressure constraint at each gas node is described as:

$$\underline{pr}_m \leq pr_{m,t} \leq \bar{pr}_m \quad (27)$$

where $pr_{m,t}$ is the pressure of gas node m at time t ; and \underline{pr}_m and \bar{pr}_m are the lower and upper limits of $pr_{m,t}$, respectively.

In (28), the gas flow is given by the Weymouth equation [32]. Also, the gas flow can be calculated by the average inflow and outflow along a pipeline in (29).

$$pr_{m,t}^2 - pr_{n,t}^2 = k_{m,n} Q_{m,n,t} |Q_{m,n,t}| \quad (28)$$

where $k_{m,n}$ is the gas flow constant of the pipeline from node m to node n ; and $Q_{m,n,t}$ is the gas flow in pipeline mn at time t .

Considering the direction of the gas flow, a binary variable is introduced to denote the flow direction, where $y_{mn} = 1$ signifies the gas flow from node m to n , and $y_{mn} = 0$ indicates the opposite gas flow direction. Therefore, the gas flow of pipelines can be described as:

$$Q_{m,n,t} = Q_{m,n,t}^+ - Q_{m,n,t}^- \quad (29)$$

$$Q_{m,n,t}^+ = \frac{Q_{m,n,t}^{\text{in}} + Q_{m,n,t}^{\text{out}}}{2} \quad (30)$$

$$Q_{m,n,t}^- = \frac{Q_{m,n,t}^{\text{in}} - Q_{m,n,t}^{\text{out}}}{2} \quad (31)$$

$$0 \leq Q_{m,n,t}^+ \leq Q_{m,n}^{\text{max}} y_{mn} \quad (32)$$

$$0 \leq Q_{m,n,t}^- \leq Q_{m,n}^{\text{max}} (1 - y_{mn}) \quad (33)$$

where $Q_{m,n,t}^{\text{in}}$ and $Q_{m,n,t}^{\text{out}}$ are the inflow and outflow gas flows of pipeline mn at time t , respectively; $Q_{m,n,t}^+$ and $Q_{m,n,t}^-$ are the forward and reverse flows of pipeline mn at time t , respectively; $Q_{m,n,t}^{\text{in}}$ and $Q_{m,n,t}^{\text{out}}$ are the reverse and forward flows of pipeline mn at time t , respectively; and $Q_{m,n}^{\text{max}}$ is the maximum gas flow of pipeline mn .

The line pack storage is calculated by the inflow and the outflow of the pipeline in (34). Meanwhile, as shown in (35), the line pack is related to the pressures at both ends of the pipeline. Constraint (36) defines that the initial line pack at the beginning of the optimization is equal to that at the end of the optimization.

$$H_{m,n,t} = H_{m,n,t-1} + (Q_{m,n,t}^{\text{in}} - Q_{m,n,t}^{\text{out}}) \quad (34)$$

$$H_{m,n,t} = S_{m,n} \frac{pr_{m,t} + pr_{n,t}}{2} \quad (35)$$

$$H_{m,n}^0 \leq H_{m,n,T} \quad (36)$$

where $H_{m,n,t}$ and $H_{m,n,t-1}$ are the stored mass of natural gas (line pack) in pipeline mn at time t and $t-1$, respectively; $S_{m,n}$ is the line pack constant of pipeline mn ; $H_{m,n}^0$ is the initial line pack of pipeline mn ; and $H_{m,n,T}$ is the line pack of pipeline mn at the end of the planning time period.

Similar to the reformulated power constraints in Section III-B using symmetrical SOCP, sequential SOCP will be applied to the constraints of natural gas.

The natural gas model shown above is nonlinear and non-convex, resulting from the nonlinearity of the gas flow equation in (28). Thus, auxiliary variables, \mathcal{O}_{mn} , pr_m^{Aux} , and pr_n^{Aux} , are utilized to form the reformulated equations [25] as:

$$\mathcal{O}_{mn} = k_{m,n} Q_{mn}^2 \quad (37)$$

$$pr_m^{\text{Aux}} = pr_m^2 \quad (38)$$

$$\mathcal{O}_{mn} = |pr_m^{\text{Aux}} - pr_n^{\text{Aux}}| \quad (39)$$

where $k_{m,n}$ is the coefficient of pipeline mn .

Then, the convex constraints of (37) and (38) are expressed in (40) and (41), respectively.

$$\mathcal{O}_{mn} \geq k_{m,n} Q_{mn}^2 \quad (40)$$

$$pr_m^{\text{Aux}} \geq pr_m^2 \quad (41)$$

Similarly, the concave constraints of (37) and (38) are shown below:

$$\mathcal{O}_{mn} \leq k_{m,n} Q_{mn}^2 \quad (42)$$

$$pr_m^{\text{Aux}} \leq pr_m^2 \quad (43)$$

Equation (39) is converted into equivalent convex and concave forms.

$$\mathcal{O}_{mn} \geq pr_n^{\text{Aux}} - pr_m^{\text{Aux}} + 2y_{mn} (pr_m^{\text{Aux}, \text{min}} - pr_n^{\text{Aux}, \text{max}}) \quad (44)$$

$$\mathcal{O}_{mn} \geq pr_m^{\text{Aux}} - pr_n^{\text{Aux}} + (2y_{mn} - 2)(pr_m^{\text{Aux}, \text{max}} - pr_n^{\text{Aux}, \text{min}}) \quad (45)$$

$$\mathcal{O}_{mn} \leq pr_n^{\text{Aux}} - pr_m^{\text{Aux}} + 2y_{mn} (pr_m^{\text{Aux}, \text{max}} - pr_n^{\text{Aux}, \text{min}}) \quad (46)$$

$$\varnothing_{mn} \leq pr_m^{Aux} - pr_n^{Aux} + (2y_{mn} - 2)(pr_m^{Aux, \min} - pr_n^{Aux, \max}) \quad (47)$$

where $pr_m^{Aux, \min}$ and $pr_m^{Aux, \max}$ are the minimum and maximum values of pr_m^{Aux} , respectively.

Consequently, the constraints of pressure of pipelines are defined as:

$$(1 - y_{mn})(pr_m^{Aux, \min} - pr_n^{Aux, \max}) \leq pr_m^{Aux} - pr_n^{Aux} \leq y_{mn}(pr_m^{Aux, \max} - pr_n^{Aux, \min}) \quad (48)$$

$$(1 - y_{mn})\left(pr_{m,t}^2 - (pr_{n,t}^{Aux, \max})^2\right) \leq pr_{m,t}^2 - pr_{n,t}^2 \leq y_{mn}\left((pr_{m,t}^{Aux, \max})^2 - (pr_{n,t}^{Aux, \min})^2\right) \quad (49)$$

Because of the inherent inaccuracy of the relaxation of (40) and (41), a sequential solution method is employed to guarantee the tightening of gas constraints. This method permits initial violations during the beginning iterations. As iterations go, the feasible range of relaxation incrementally converges towards that of the original problem, achieved by introducing penalties on the constraints that may be violated.

The sequential SOCP solution method is applied to tighten (40) and (41). The convergence of sequential SOCP has been proven by [33]. Taylor expansion is used to linearize constraints (42) and (43).

$$\varnothing_{mn} \leq k_{m,n} \left(2Q_{m,n}^{(ite-1)} Q_{m,n} - (Q_{m,n}^{(ite-1)})^2 \right) + \alpha_{mn} \quad (50)$$

$$pr_m^{Aux} \leq 2pr_m^{Aux, (ite-1)} pr_m^{Aux} - (pr_m^{Aux, (ite-1)})^2 + \delta_{mn} \quad (51)$$

where α_{mn} and δ_{mn} are the non-negative slack variables; and $Q_{m,n}^{(ite-1)}$ and $pr_m^{Aux, (ite-1)}$ are the values of $Q_{m,n}$ and pr_m^{Aux} in the last iteration, respectively.

D. GFPP Constraints

The capacity constraint of GFPP is given as (52). As the GFPPs inject three-phase power into the three-phase power grid, constraints (53) and (54) guarantee that the outputs of three phases have the same values of both active power and reactive power, respectively.

$$\sqrt{(P_{i,t}^{GFPP})^2 + (Q_{i,t}^{GFPP})^2} \leq S_i^{GFPP} \quad (52)$$

$$P_{a,i,t}^{GFPP} = P_{b,i,t}^{GFPP} = P_{c,i,t}^{GFPP} \quad (53)$$

$$Q_{a,i,t}^{GFPP} = Q_{b,i,t}^{GFPP} = Q_{c,i,t}^{GFPP} \quad (54)$$

where the subscripts a and b represent the phases a and b , respectively; $P_{i,t}^{GFPP}$ and $Q_{i,t}^{GFPP}$ are the active power and reactive power of GFPP at node i at time t , respectively; and S_i^{GFPP} is the capacity of GFPP at node i .

An SOCP model is employed for (52). Within SOCP, an inequality can be relaxed to an equation, because the optimizer is inherently capable of identifying the tightest limit within the allowable range. This relaxation makes the problem more tractable without sacrificing the optimal solution.

$$\left\| \begin{matrix} P_{i,t}^{GFPP} \\ Q_{i,t}^{GFPP} \end{matrix} \right\|_2 \leq S_i^{GFPP} \quad (55)$$

E. P2G Unit Constraints

The capacity constraint of the P2G unit is expressed as

(56). Constraint (57) defines the relation between active power input and reactive power input of the P2G unit.

As the P2G unit takes the electric energy from the three-phase power grid, constraint (58) imposes that the power inputs from three phases have the same value. As shown in (59), the natural gas output of P2G is proportional to its active power input.

$$\sqrt{(P_{i,t}^{P2G})^2 + (Q_{i,t}^{P2G})^2} \leq S_i^{P2G} \quad (56)$$

$$Q_{i,t}^{P2G} = P_{i,t}^{P2G} \tan \theta_{i,t}^{P2G} \quad (57)$$

$$P_{a,i,t}^{P2G} = P_{b,i,t}^{P2G} = P_{c,i,t}^{P2G} = \frac{P_{i,t}^{P2G}}{3} \quad (58)$$

$$G_{n,t}^{P2G} = \eta^{P2G} \varnothing^{P2G} P_{i,t}^{P2G} \quad (59)$$

where $P_{i,t}^{P2G}$ and $Q_{i,t}^{P2G}$ are the active power and the reactive power of P2G at node i at time t , respectively; S_i^{P2G} is the capacity of power input of P2G; $\theta_{i,t}^{P2G}$ is the power factor of P2G; $P_{a,i,t}^{P2G}$, $P_{b,i,t}^{P2G}$, and $P_{c,i,t}^{P2G}$ are the active power of P2G unit in phases a , b , and c of node i at time t , respectively; $G_{n,t}^{P2G}$ is the natural gas output of P2G at node n of the natural gas network at time t ; \varnothing^{P2G} is the energy conversion factor of natural gas and electric power (kcf/MWh); and η^{P2G} is the energy efficiency of P2G.

When applying the sequential SOCP model, (56) is converted to the constraint shown in (60).

$$\left\| \begin{matrix} P_{i,t}^{P2G} \\ Q_{i,t}^{P2G} \end{matrix} \right\|_2 \leq S_i^{P2G} \quad (60)$$

The flowchart of the SS-SOCP method is shown in Fig. 2, which outlines the solving steps of an SS-SOCP problem for optimization of MES. This method can ensure that all constraints of the MES are met, and a feasible optimal solution is obtained.

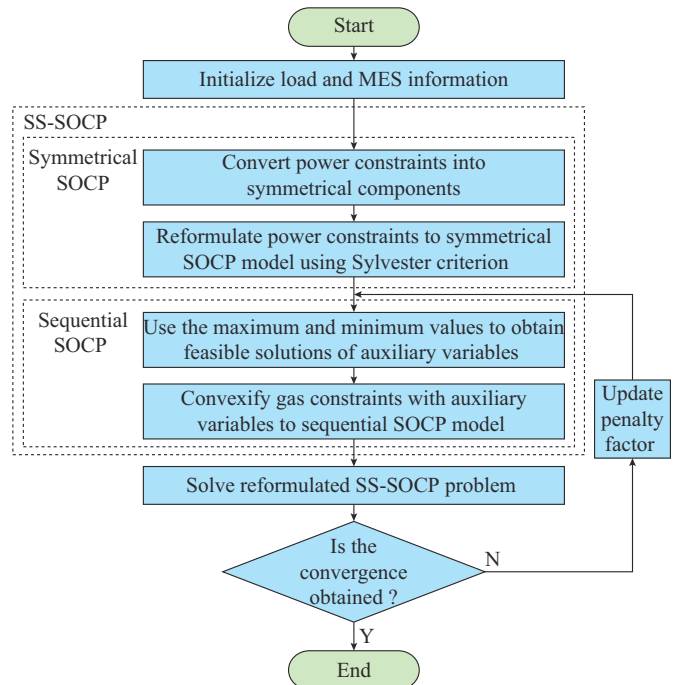


Fig. 2. Flowchart of SS-SOCP method.

IV. CASE STUDY

The optimization program for case studies in this section is coded in YALMIP [34] and solved by MOSEK in MATLAB R2018a, with an operational environment of Windows 10 Intel i7-7700HQ CPU of 2.80 GHz and 16 GB of RAM.

A. Test Case and Scenarios

As shown in Fig. 3, an MES, consisting of a modified

IEEE 123-node power distribution system with a 20-node natural gas network through two GFPPs and a P2G unit, is built to verify the effectiveness of the operational coordination optimization method for ENG-MES. The method aims to minimize the total operational cost, maximize the utilization of the installed wind power, and reduce the overall carbon emissions. The profiles of electric power loads, natural gas loads, and wind power generation are shown in Fig. 4.

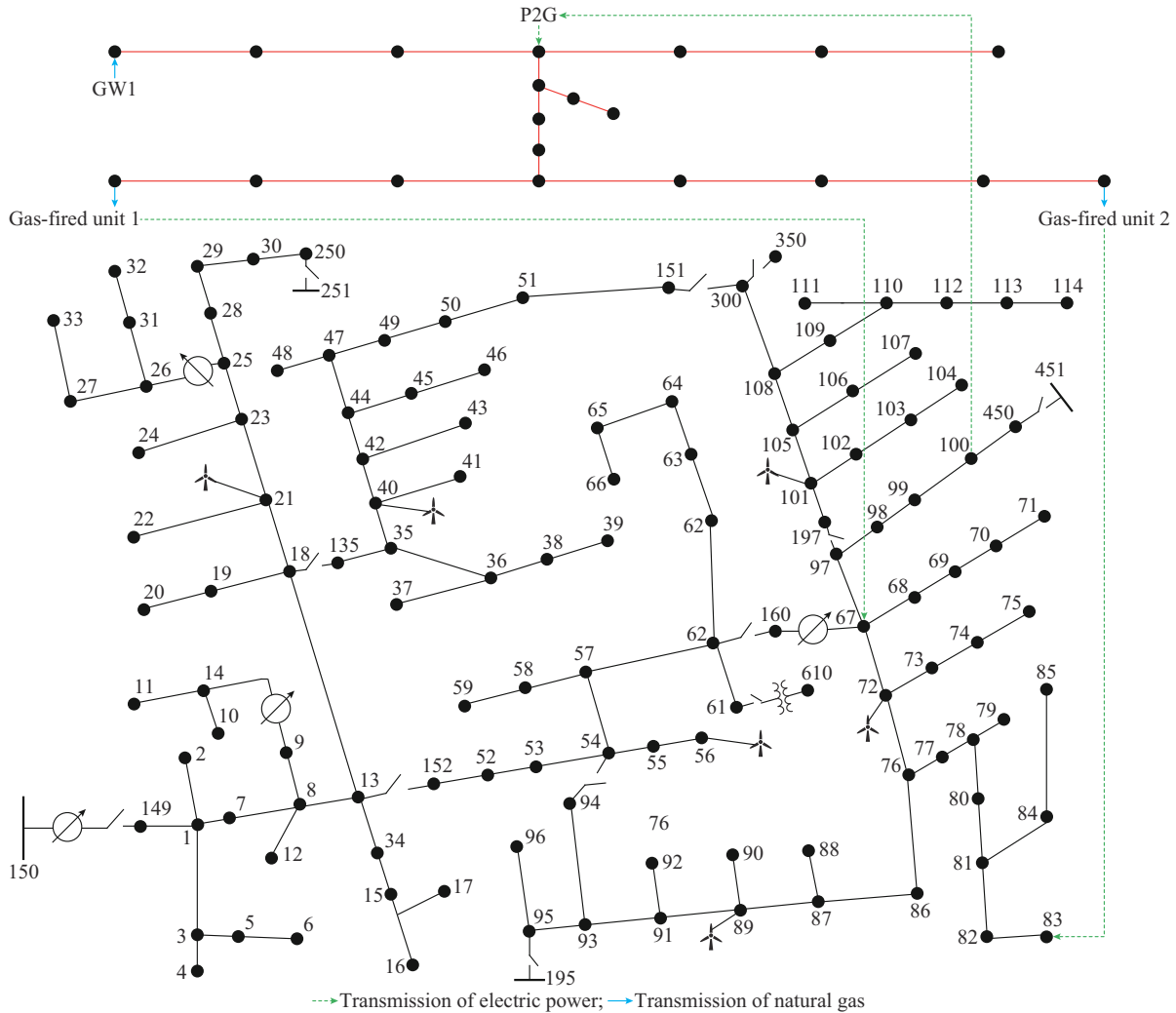


Fig. 3. Illustration of MES for case studies.

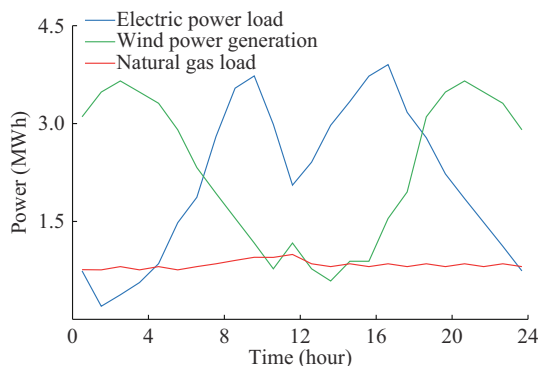


Fig. 4. Profiles of electric power loads, natural gas loads, and wind power generation.

In the electricity network, the rated voltage is 4.16 kV with the minimum and maximum voltage limits set as 0.95 p.u. and 1.05 p.u., respectively. The total active and reactive power of the electric power loads in the network is 3490 kW and 1920 kvar, respectively [35].

To further investigate the role of P2G in the accommodation of REG, six wind power units are integrated into the electricity network and operated with a constant power factor of 1.0. Each wind power unit has a capacity of 600 kVA and the location information of each unit is shown in Fig. 3. It is assumed that all the power from the upstream power grid (node 150) is generated by coal-fired power plants.

In the natural gas network with the aforementioned parameters [11], the GFPPs are located at electric nodes 67 and

83, respectively, and take natural gas as fuel from gas nodes 20 and 12. The P2G unit gets electricity from electric node 100 and sends the produced natural gas to the gas network through gas node 4. Two GWs are located at gas nodes 1 and 15.

Three scenarios are designed and implemented in the case studies to analyze the benefits of the operational coordination optimization method for ENG-MES.

1) Scenario I: separate operations of the electricity network and the natural gas network without participation of the GFPPs and the P2G unit.

2) Scenario II: coordinated operation only with the GFPPs.

3) Scenario III: coordinated operation, considering bidirectional energy flow through the GFPPs and the P2G unit.

Scenario I is the foundational base case, reflecting the traditional energy management practices. Each network is optimized separately without considering potential benefits gained from coordination. In Scenario II, the networks include coordinated operations involving GFPPs, to explore the initial steps towards the ENG-MES by examining the impacts of GFPPs through the comparison with Scenario I. Scenario III is designed for the full coordinated operation of MES by enabling both GFPPs and P2G.

B. Analysis of Optimization Results

The results of the case studies in three scenarios are shown in Table I. The comparison of the results in three scenarios is presented in Fig. 5.

TABLE I
RESULTS OF CASE STUDIES IN THREE SCENARIOS

Scenario	Operational cost (\$)	Curtailed wind power generation (MWh)	Carbon emission (t)
I	1319.15	24.17	16.67
II	1221.33	24.21	12.34
III	1065.22	1.35	11.07

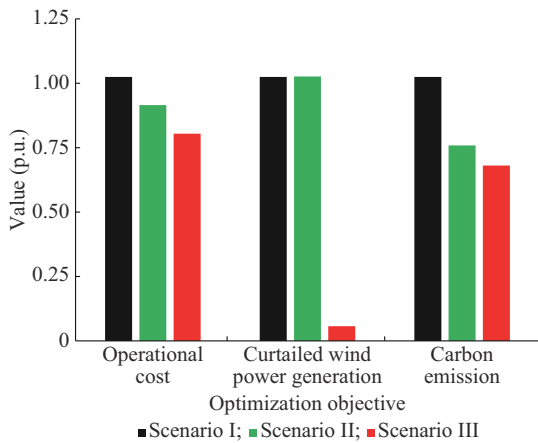


Fig. 5. Comparison of results in three scenarios.

In Scenario I, the curtailed wind power generation (24.17 MWh) is up to 44.24% of all available wind power generation (54.63 MWh). The total operational cost is \$1319.15 and the overall carbon emission is 16.67 t.

In Scenario II, the curtailed wind power generation (24.21 MWh) remains almost the same as that in Scenario I. However, the total operational cost achieves a 7.42% reduction from \$1319.15 to \$1221.33 compared with that in Scenario I. Meanwhile, the overall carbon emission is reduced by 25.96% from 16.67 t to 12.34 t from that of Scenario I.

In Scenario III, compared with those in Scenarios I and II, the curtailed wind power generation is greatly decreased by 94.40%; the total operational cost becomes 19.25% less than that in Scenario I and 12.78% less than that in Scenario II. The overall carbon emission is 33.59% less than that in Scenario I and 10.29 % less than that in Scenario II.

As the coal-fired power plants (870 g/kWh) have nearly twice the carbon emission as the gas-fired counterparts (401 g/kWh) [36], in Scenarios II, the electricity from GFPPs can replace a part of the electricity from coal-fired power plants, resulting in a notable reduction of carbon emission in Scenario II compared with that in Scenario I. Furthermore, in Scenario III, because of the engagement of P2G unit, a further reduction of carbon emissions is achieved by the increasing integration of wind power.

C. Technical Benefit Comparison of Three Scenarios from Electricity Profiles

The hourly profiles of electricity in the power distribution system for the three scenarios are shown in Fig. 6.

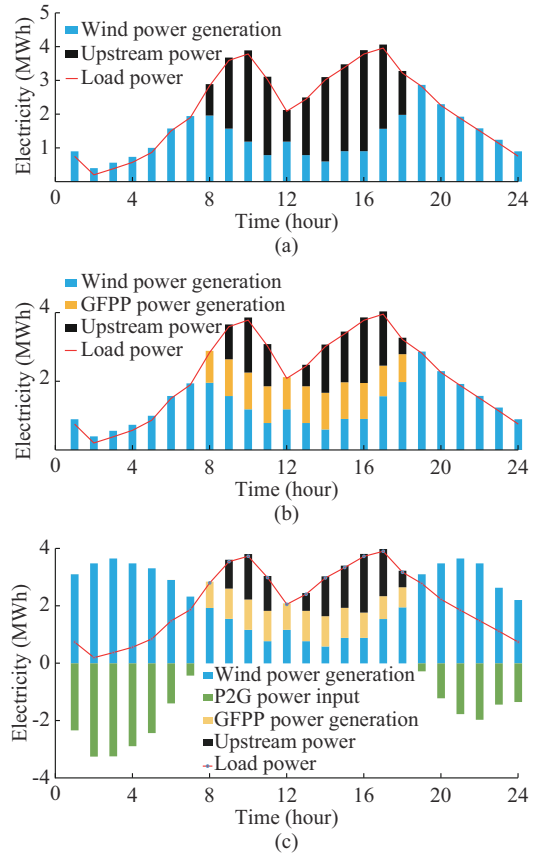


Fig. 6. Hourly profiles of electricity. (a) Scenario I. (b) Scenario II. (c) Scenario III.

In Scenario I, as the electricity network and the natural gas network operate independently, the electricity demand of

loads is satisfied by the power from both the upstream grids and the generation of wind power in the power distribution system. As shown in Fig. 6(a), during hours 1-7 and hours 19-24, all the electric power loads are powered by wind power generation, while during hours 8-18, due to the insufficient wind power generation, the upstream power is required to meet the demand of electric power loads together with the low wind power generation during that period. In the absence of an energy storage system in the power distribution system, it is inevitable that surplus wind power generation will be curtailed and thus wasted when wind power generation exceeds the demand for electricity.

In Scenario II, according to Table II and Fig. 6(b), with the engagement of the GFPPs, the electricity demand is covered by both the upstream power (50.69%) and the GFPP power generation (49.31%). The upstream power is reduced from 21.93 MWh to 11.02 MWh. Meanwhile, the GW output increases by 201.07% from 67.47 kcf to 203.13 kcf. The increased amount of natural gas is used as the fuel of GFPPs. As shown in Fig. 6(b), during hours 1-7 and hours 19-24, all the electric power loads are also supplied by the wind power generation, which is the same as those in Scenario I. However, during hours 8-18, compared with Scenario I of Fig. 6(a), nearly half of the upstream power is replaced by the GFPP power generation.

TABLE II
ELECTRICITY AND NATURAL GAS STATUS FOR THREE SCENARIOS

Scenario	Upstream power (MWh)	GW output (kcf)	GFPP power generation (MWh)	P2G gas output (kcf)
I	21.93	74.22	N/A	N/A
II	11.02	223.44	10.72	N/A
III	11.37	165.57	10.38	48.29

In Scenario III, the upstream power and the GFPP power generation are close to those in Scenario II. However, from the comparison of Fig. 6(b) and (c), the wind power generation in Scenario III is largely greater than that in Scenario II, which is also shown by the data of the curtailed wind power generation in Table I. In Fig. 6(c), when the wind power generation is excessive during hours 1-7 and hours 19-24, the P2G unit is deployed to operate. In contrast, when the wind power generation is insufficient to meet the electricity demand during the hours 8-18, the P2G unit stops working.

D. Integration of Wind Power Generation

Figure 7 presents a comparison of wind power accommodation in three scenarios. The output profiles of wind power generation in Scenarios I and II exhibit a high degree of similarity with a certain amount of wind power curtailment. In contrast, in Scenario III, the output of the wind power generation almost matches the curve of the available wind power generation, as the P2G unit can serve as a controllable load in the electricity network and convert the surplus wind power generation into the natural gas stored in pipelines.

As illustrated in Fig. 7 and Table II, in Scenario III, approximately 1.35 MWh of the available wind power genera-

tion is curtailed at hours 23 and 24. According to (36), the line pack in pipelines at the end of the optimization period is equal to that at the beginning. Therefore, the operation of the P2G unit can reduce the curtailed wind power, yet there may still be a certain amount of wind power generation wasted.

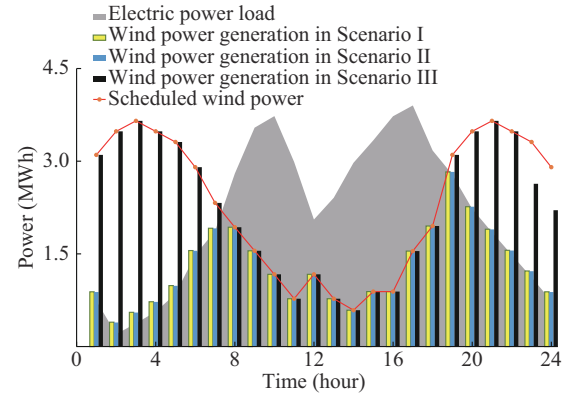


Fig. 7. Comparison of wind power accommodation in three scenarios.

The P2G unit only operates in Scenario III. P2G consumes the surplus wind power to maximize the integration of wind power generation. Without P2G, the surplus wind power should be curtailed due to capacity limits of the power system.

E. Three-phase Voltage Imbalance

In the case studies, the three-phase power distribution system is modeled, and the unbalanced condition of the three-phase voltage at each node is also evaluated by using the voltage unbalanced factor (VUF) as:

$$VUF = \frac{\sum_{t=0}^T \sum_{i=1}^N |V_{i,t,-}|^2}{|V_{i,t,+}|^2} \quad (61)$$

$$V_{i,t,+} = \frac{1}{3} (V_{i,t}^a + \alpha^2 V_{i,t}^b + \alpha V_{i,t}^c) \quad (62)$$

$$V_{i,t,-} = \frac{1}{3} (V_{i,t}^a + \alpha V_{i,t}^b + \alpha^2 V_{i,t}^c) \quad (63)$$

where $V_{i,t,+}$ is the positive-sequence voltage at node i at time t ; $V_{i,t,-}$ is the negative-sequence voltage at node i at time t ; and $\alpha = 1 \angle 120^\circ$.

The three-phase voltage imbalance in the three scenarios is presented in Fig. 8.

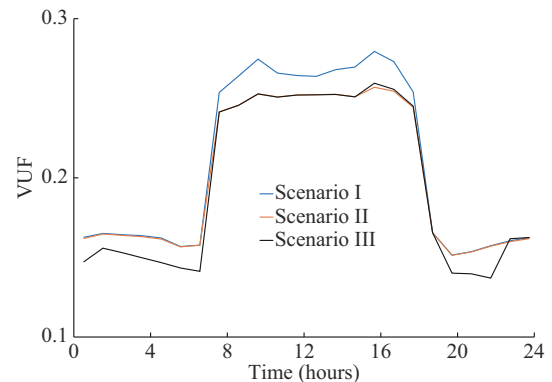


Fig. 8. Three-phase voltage imbalance in three scenarios.

During the period with high electric power load, the three-phase voltage imbalance deteriorates, and vice versa. Compared with Scenario I, the three-phase voltage imbalance is mitigated in both Scenarios II and III. Meanwhile, with the application of the P2G unit, Scenario III achieves a further improvement in the three-phase voltage imbalance than Scenario II. Therefore, the establishment of an ENG-MES can also contribute to the mitigation of the three-phase voltage imbalance in the electricity network.

F. Technical Benefit Comparison of Three Scenarios from Natural Gas Profile

Figure 9 shows the hourly profiles of natural gas in Scenarios II and III. In Scenario II, from hours 1 to 9, the two GWs inject natural gas into the pipelines. The GFPPs generate power during the period of daytime peak load. Also, part of the natural gas is injected into pipelines near the end of the day (hours 22-24), as the constraint guarantees that during the optimization period, the initially stored mass at the beginning has the same amount as that at the end.

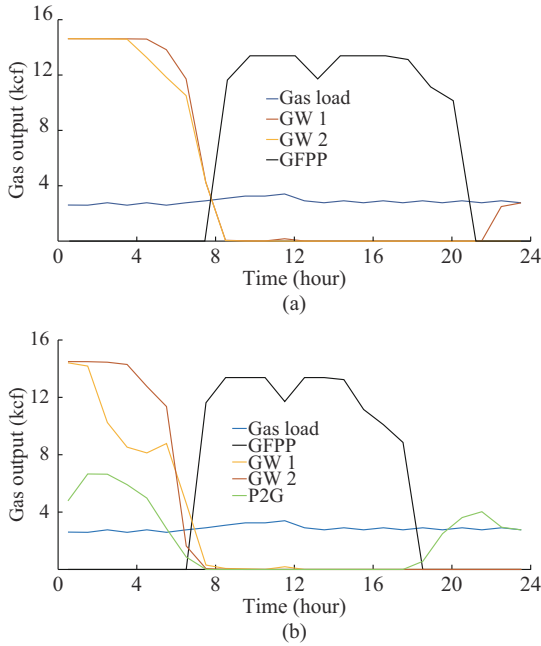


Fig. 9. Hourly profiles of natural gas in Scenarios II and III. (a) Scenario II. (b) Scenario III.

According to Table I and Fig. 9, because of the operation of the P2G unit, the gas output of the GWs in Scenario III (165.57 kecf) is 25.90% lower than that in Scenario II (223.44 kecf). Also, the GWs in Scenario III do not have gas output near the end of the day (hours 22-24) as in Scenario II. Therefore, during the evening time of hours 19-24, the P2G converts the surplus wind power generation to natural gas. The gas output profile of the P2G unit in Fig. 9(b) corresponds to the P2G power input in Fig. 6(c).

The dynamics of the pipeline are shown in Fig. 10. According to Fig. 4, in both Fig. 10(a) and (b), the periods of pipeline charging exactly correspond to those when the wind power generation is greater than the electric power loads, as the P2G unit can only convert the excess wind power genera-

tion into natural gas. In the instances where the wind power generation is insufficient to meet the demands of electric power loads, the P2G unit is deactivated and the GFPPs engage in wind power generation by using natural gas as fuel. This subsequently results in a discharge of natural gas from the pipelines.

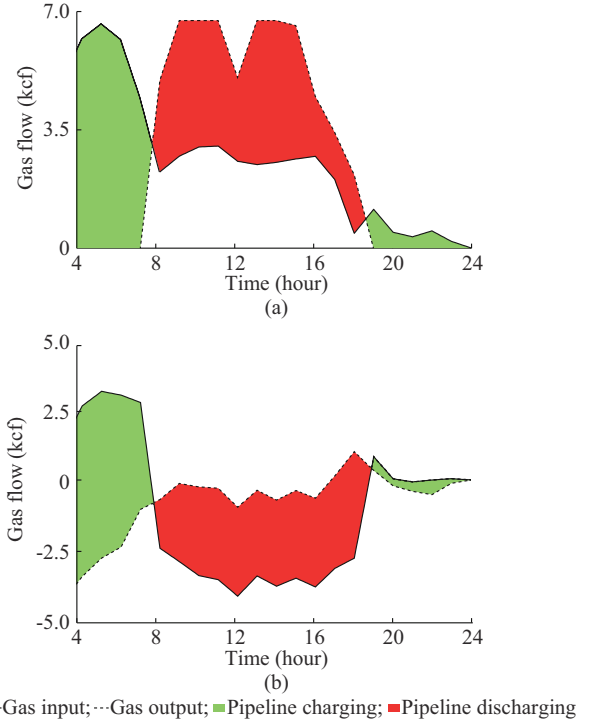


Fig. 10. Dynamics of pipeline. (a) Between gas nodes 5 and 6. (b) Between gas nodes 3 and 5.

In Fig. 10(a), the values of both the curve of pipeline charging (solid line) and discharging (dash line) are greater than or equal to 0, meaning that all the natural gas in the pipeline between gas nodes 5 and 6 is only charged through gas node 5 and discharged through gas node 6. On the contrary, in the pipeline between gas nodes 3 and 5 in Fig. 10 (b), the charging and discharging of the natural gas occur at both two nodes.

By converting surplus REG into natural gas and storing it in the pipelines, the P2G unit can charge the pipelines because of the dynamic line pack of the pipeline. Meanwhile, GFPPs can generate electricity for electricity networks using natural gas stored in pipelines. As a result, the natural gas network can serve as an energy storage system for electric power.

G. Algorithm Verification and Comparison

As shown in Table III, four various methods are compared, each representing a distinct combination of algorithms. To validate the accuracy and computational efficiency of the SS-SOCP, the discrepancies of power flow and voltage are calculated in (64) and (65), respectively, while the violation of gas flow is defined in (66).

$$\Delta_S = \sum \text{diag} \left(A \left(S_{j,t}^{012} - z_{j,t}^{012} I_{j,t}^{012} \right) A^H \right) + s_{j,t} + y_{i,t}^{012} v_{i,t}^{012} - \sum \text{diag} \left(A S_{j,t}^{012} A^H \right) \quad (64)$$

$$\Delta_v = \mathbf{v}_{j,t}^{012} - \mathbf{v}_{i,t}^{012} + \left(\mathbf{S}_{ij,t}^{012} \left(\mathbf{z}_{ij,t}^{012} \right)^H + \left(\mathbf{S}_{ij,t}^{012} \right)^H \mathbf{z}_{ij,t}^{012} \right) - \mathbf{z}_{ij,t}^{012} \mathbf{I}_{ij,t}^{012} \left(\mathbf{z}_{ij,t}^{012} \right)^H \quad (65)$$

$$\Delta_G = \frac{\left| pr_{m,t}^2 - pr_{n,t}^2 - k_{m,n} Q_{m,n,t} \right| Q_{m,n,t}}{k_{m,n} Q_{m,n,t} \left| Q_{m,n,t} \right|} \quad (66)$$

where Δ_s represents the difference between power inflows and outflows; Δ_v represents the voltage difference along branch ij ; and Δ_G represents the violation in gas flow. For Δ_s , Δ_v , and Δ_G , a value approaching zero suggests a global optimal solution.

TABLE III
COMBINATION OF VARIOUS METHODS FOR COMPARISON

Method	Algorithm for power constraint	Algorithm for gas constraint
Method 1 [37]	Linear	Mix-integer linear
Method 2 [38]	Linear	Sequential SOCP
Method 3 [38]	SOCP	Sequential SOCP
Proposed SS-SOCP Method	Symmetrical SOCP	Sequential SOCP

From the comparative analysis of various methods presented in Table IV, method 1 has the shortest solving time of 12.96 s but exhibits high values for $|\Delta_s|$, $|\Delta_v|$, and $|\Delta_G|$. The linear method without containing square terms can simplify and accelerate the solving process, while this kind of simplification results in lower stability and accuracy. As sequential SOCP has been proven effective and accurate in achieving optimal results of gas constraints, the values of $|\Delta_G|$ in methods 2, 3, and the proposed SS-SOCP method approaches zero, indicating highly accurate optimal results. In method 3, SOCP overlooks the coupling between three phases, leading to varying degrees of inaccuracy in the optimization results. Therefore, compared with the proposed SS-SOCP method, the inaccuracy is shown in the optimization results of the three-phase power systems. The proposed SS-SOCP method stands out with a solving time of 25.13 s, achieving the most remarkable reduction in all stability and accuracy indexes: $|\Delta_s|$ is minimized to 1.78×10^{-3} , $|\Delta_v|$ is minimized to 6.67×10^{-7} , while maintaining a low $|\Delta_G|$ of 2.50×10^{-4} . The proposed SS-SOCP method clearly demonstrates superior performance in terms of producing precise solutions, even without the fastest solving time. In summary, compared with other methods, the proposed SS-SOCP method can be selected as a balanced option with nearly the lowest solving time and highest accuracy.

TABLE IV
COMPARISON OF ACCURACY AND SOLVING TIME FOR VARIOUS METHODS

Method	Solving time (s)	$ \Delta_s $	$ \Delta_v $	$ \Delta_G $
Method 1 [37]	12.96	205.01	7.31	1.20×10^{-1}
Method 2 [38]	18.72	204.66	5.56	2.61×10^{-4}
Method 3 [38]	31.87	23.43	4.80×10^{-1}	2.53×10^{-4}
Proposed SS-SOCP Method	25.13	1.78×10^{-3}	6.67×10^{-7}	2.50×10^{-4}

V. CONCLUSION

In this paper, an operational optimization method for the ENG-MESs, having bi-directional energy flows through P2G and GFPPs, is designed and developed with detailed modelling of electricity network and natural gas network. The employment of the SS-SOCP enables the conversion of a complex, non-convex, and nonlinear model into a solvable model. It is proven that the SS-SOCP method can be used in the modelling and optimization of a three-phase power systems and then MES, which brings the three-phase analysis of the power systems into the coupling of multiple energy vectors.

The results of the case studies indicate that the proposed operational coordination optimization method for ENG-MES is effective in jointly minimizing the operational cost, limiting the curtailment of wind power, mitigating the voltage imbalance, and reducing the carbon emission. Also, it is proven that P2G can release system flexibility and benefit the economy by economically managing the carbon footprint of the entire system, via converting excess “green” electricity into natural gas which can be injected and stored into pipelines. The proposed operational coordination optimization method for ENG-MES demonstrates this potential of coupling method in addressing two critical challenges: the efficient integration of REG and the reduction of three-phase voltage imbalance, which are prevalent issues in the power distribution system.

Future work can incorporate uncertainty analysis to tackle the variability of renewable energy sources, enhancing the robustness and real-world applicability of the energy coupling method.

REFERENCES

- [1] W. Wang, S. Huang, G. Zhang *et al.*, “Optimal operation of an integrated electricity-heat energy system considering flexible resources dispatch for renewable integration,” *Journal of Modern Power Systems and Clean Energy*, vol. 9, no. 4, pp. 699-710, Jul. 2021.
- [2] C. Andrade, S. Seloisse, and N. Maïzi, “The role of power-to-gas in the integration of variable renewables,” *Applied Energy*, vol. 313, p. 118730, May 2022.
- [3] M. Lynch, M. T. Devine, and V. Bertsch, “The role of power-to-gas in the future energy system: market and portfolio effects,” *Energy*, vol. 185, pp. 1197-1209, Jan. 2019.
- [4] Y. Jiang, J. Xu, Y. Sun *et al.*, “Coordinated operation of gas-electricity integrated distribution system with multi-CCHP and distributed renewable energy sources,” *Applied Energy*, vol. 211, p. 23748, Feb. 2018.
- [5] A. R. Sayed, C. Wang, J. Zhao *et al.*, “Distribution-level robust energy management of power systems considering bidirectional interactions with gas systems,” *IEEE Transactions on Smart Grid*, vol. 11, no. 3, pp. 2092-2105, May 2020.
- [6] C. Wang, R. Zhang, and T. Bi, “Energy management of distribution-level integrated electric-gas systems with fast frequency reserve,” *IEEE Transactions on Power Systems*, vol. 39, no. 2, pp. 4208-4223, Mar. 2024.
- [7] F. Qi, M. Shahidehpour, F. Wen *et al.*, “Decentralized privacy-preserving operation of multi-area integrated electricity and natural gas systems with renewable energy resources,” *IEEE Transactions on Sustainable Energy*, vol. 11, no. 3, pp. 1785-1796, Jul. 2020.
- [8] F. Qi, M. Shahidehpour, Z. Li *et al.*, “A chance-constrained decentralized operation of multi-area integrated electricity-natural gas systems with variable wind and solar energy,” *IEEE Transactions on Sustainable Energy*, vol. 11, no. 4, pp. 2230-2240, Oct. 2020.
- [9] L. Yang, Y. Xu, W. Gu *et al.*, “Distributionally robust chance-constrained optimal power-gas flow under bidirectional interactions considering uncertain wind power,” *IEEE Transactions on Smart Grid*, vol. 12, no. 2, pp. 1722-1735, Mar. 2021.
- [10] S. Chen, A. J. Conejo, R. Sioshansi *et al.*, “Unit commitment with an enhanced natural gas-flow model,” *IEEE Transactions on Power Sys-*

- tems*, vol. 34, no. 5, pp. 3729-3738, Sept. 2019.
- [11] A. Schwele, A. Arrigo, C. Vervaeren *et al.*, "Coordination of electricity, heat, and natural gas systems accounting for network flexibility," *Electric Power Systems Research*, vol. 189, p. 106776, Dec. 2020.
- [12] K. P. Schneider, B. A. Mather, B. C. Pal *et al.*, "Analytic considerations and design basis for the IEEE distribution test feeders," *IEEE Transactions on Power Systems*, vol. 33, no. 3, pp. 3181-3188, May 2018.
- [13] R. Jabr, "Exploiting sparsity in SDP relaxations of the OPF problem," *IEEE Transactions on Power Systems*, vol. 27, no. 2, pp. 1138-1139, May 2012.
- [14] S. Bruno, S. Lamonaca, G. Rotondo *et al.*, "Unbalanced three-phase optimal power flow for smart grids," *IEEE Transactions on Industrial Electronics*, vol. 58, no. 10, pp. 4504-4513, Oct. 2011.
- [15] E. Dall'Anese, H. Zhu, and G. B. Giannakis, "Distributed optimal power flow for smart microgrids," *IEEE Transactions on Smart Grid*, vol. 4, no. 3, pp. 1464-1475, Sept. 2013.
- [16] S. H. Low, "Convex relaxation of optimal power flow – part I: formulations and equivalence," *IEEE Transactions on Control of Network Systems*, vol. 1, no. 1, pp. 15-27, Mar. 2014.
- [17] Z. Wang, D. S. Kirschen, and B. Zhang. (2017, Dec.). Accurate semidefinite programming models for optimal power flow in distribution systems. [Online]. Available: <https://ui.adsabs.harvard.edu/abs/2017arXiv171107853W/abstract>
- [18] E. Dall'Anese, H. Zhu, and G. B. Giannakis, "Distributed optimal power flow for smart microgrids," *IEEE Transactions on Smart Grid*, vol. 4, no. 3, pp. 1464-1475, Sept. 2013.
- [19] L. Gan, N. Li, U. Topcu *et al.*, "Exact convex relaxation of optimal power flow in radial networks," *IEEE Transactions on Automatic Control*, vol. 60, no. 1, pp. 72-87, Jan. 2015.
- [20] C. Lou, L. Zhang, W. Tang *et al.*, "A coordinated restoration method of three-phase AC unbalanced distribution network with DC connections and mobile energy storage systems," *International Journal of Electrical Power and Energy Systems*, vol. 157, p. 109895, Feb. 2024.
- [21] S. Chen, A. J. Conejo, R. Sioshansi *et al.*, "Unit Commitment with an enhanced natural gas-flow model," *IEEE Transactions on Power Systems*, vol. 34, no. 5, pp. 3729-3738, Sept. 2019.
- [22] C. Wang, W. Wei, J. Wang *et al.*, "Convex optimization based distributed optimal gas-power flow calculation," *IEEE Transactions on Sustainable Energy*, vol. 9, no. 3, pp. 1145-1156, Jul. 2018.
- [23] G. Byeon and P. van Hentenryck, "Unit commitment with gas network awareness," *IEEE Transactions on Power Systems*, vol. 35, no. 2, pp. 1327-1339, Mar. 2020.
- [24] Y. Sun, B. Zhang, L. Ge *et al.*, "Day-ahead optimization schedule for gas-electric integrated energy system based on second-order cone programming," *CSEE Journal of Power and Energy Systems*, vol. 6, no. 1, pp. 142-151, Mar. 2020.
- [25] C. Wu, W. Li, T. Qian *et al.*, "Optimal scheduling of hydrogen blended integrated electricity – gas system considering gas linepack via a sequential second-order cone programming methodology," *Journal of Energy Storage*, vol. 76, p. 109718, Nov. 2023.
- [26] A. M. Jubril, O. A. Komolafe, and K. O. Alawode, "Solving multi-objective economic dispatch problem via semidefinite programming," *IEEE Transactions on Power Systems*, vol. 28, no. 3, pp. 2056-2064, Aug. 2013.
- [27] T. L. Saaty, "Decision making – the analytic hierarchy and network processes (AHP/ANP)," *Journal of Systems Science and Systems Engineering*, vol. 13, no. 1, pp. 1-35, Mar. 2004.
- [28] A. Floriduz, M. Tucci, S. Rivero *et al.*, "Approximate Kron reduction methods for electrical networks with applications to plug-and-play control of AC islanded microgrids," *IEEE Transactions on Control Systems Technology*, vol. 27, no. 6, pp. 2403-2416, Nov. 2019.
- [29] K. P. Schneider, B. A. Mather, and B. C. Pal, "Analytic considerations and design basis for the IEEE distribution test feeders," *IEEE Transactions on Power Systems*, vol. 33, no. 3, pp. 3181-3188, May 2018.
- [30] C. Lou, J. Yang, and L. Min, "Symmetrical semidefinite programming with bifurcation phase-changing SOPs for unbalanced power distribution networks," in *Proceedings of 2021 IEEE 5th Conference on Energy Internet and Energy System Integration (EI2)*, Taiyuan, China, Oct. 2021, pp. 1242-1247.
- [31] R. A. Horn and C. R. Johnson, *Matrix Analysis*. Cambridge: Cambridge University Press, 2012.
- [32] S. R. Kazi, K. Sundar, S. Srinivasan *et al.*, "Modeling and optimization of steady flow of natural gas and hydrogen mixtures in pipeline networks," *International Journal of Hydrogen Energy*, vol. 54, pp. 14-24, Dec. 2023.
- [33] S. Wang, J. Zhai, and H. Hui, "Optimal energy flow in integrated electricity and gas systems with injection of alternative gas," *IEEE Transactions on Sustainable Energy*, vol. 14, no. 3, pp. 1540-1557, Jul. 2023.
- [34] J. Lofberg, "YALMIP: a toolbox for modeling and optimization in MATLAB," in *Proceedings of 2004 IEEE International Conference on Robotics and Automation*, Taipei, China, Sept. 2004, pp. 284-289.
- [35] P. Li, H. Ji, and C. Wang, "Coordinated control method of voltage and reactive power for active distribution networks based on soft open point," *IEEE Transactions on Sustainable Energy*, vol. 8, no. 4, pp. 1430-1442, Oct. 2017.
- [36] N. A. Odeh and T. T. Cockerill, "Life cycle analysis of UK coal fired power plants," *Energy Conversion and Management*, vol. 49, no. 2, pp. 212-220, Aug. 2008.
- [37] G. Liu, R. S. Moorthy, J. Choi *et al.*, "Linearised three-phase optimal power flow for coordinated optimisation of residential solid-state power substations," *IET Energy Systems Integration*, vol. 3, pp. 344-354, Jul. 2021.
- [38] L. Gan, N. Li, U. Topcu *et al.*, "Exact convex relaxation of optimal power flow in radial networks," *IEEE Transactions on Automatic Control*, vol. 60, no. 1, pp. 72-87, Jan. 2015.

Liang Min received the B.S. degree from Nanjing Institute of Technology, Nanjing, China, in 2017, the M.E. degree from the University of Southern California, Los Angeles, USA, in 2019, and the Ph.D. degree from the University of Glasgow, Glasgow, UK, in 2024. He is working in the Power Grid Dispatching and Control Branch Company of NARI Technology Co., Ltd., Nanjing, China. His research interests include power system modelling and optimization, and operational optimization of multi-energy system.

Chengwei Lou received the B.S. and M.E. degrees in electrical engineering and automation from China Agricultural University, Beijing, China, in 2016 and 2019, respectively, and the Ph.D. degree in electrical engineering at the University of Glasgow, Glasgow, UK, in 2022. He is currently an Associate Professor with College of Information and Electrical Engineering at the China Agricultural University. His current research interests include power distribution system modelling and optimization.

Jin Yang received the B.E. and M.Sc. degrees from North China Electric Power University, Baoding, China, in 2003 and 2006, respectively, and the Ph.D. degree from the University of Glasgow, Glasgow, UK, in 2011, all in electrical engineering. He is currently a Reader with the James Watt School of Engineering at the University of Glasgow. His current research interests include operational and optimization of power transmission and distribution network, protection of renewable power generation system, and smart grid technology.

James Yu received the Ph.D. degree in electrical engineering at the University of Newcastle, Newcastle, UK. He has worked in Scottish Power Network from 2006 and is the Leader of the future team. He is also a Research Associate at the University of Glasgow, Glasgow, UK. His research interests include innovative application of power electronics devices and optimization of power distribution network.

Zhibin Yu held positions as a Lecturer (2012-2017), Senior Lecturer (2017-2019), and Professor of Thermal Energy (2019-2023) at the James Watt School of Engineering at the University of Glasgow, Glasgow, UK. Now he is the Chair of Energy Engineering at the Department of Mechanical and Aerospace Engineering, University of Liverpool, Liverpool, UK. His research interest includes heat pump technology, thermal energy storage system, and optimization of heating network.